Heterogeneous nucleation and epitaxial crystal growth of magmatic minerals

Julia E. Hammer[1], Thomas G. Sharp[2], and Paul Wessel[1]
[1]Department of Geology and Geophysics, University of Hawaii, Hawaii 96822, USA
[2]School of Earth and Space Exploration, Arizona State University, Arizona 85287, USA

ABSTRACT

Electron backscatter diffraction analysis of dendritic clinopyroxene (cpx) forming in rapidly cooled basalt reveals two features that are unexpected for phases growing from a liquid: (1) helical growth about $\{010\}_{cpx}$, the crystallographic b-axis, with incremental rotation (up to 0.4° μm^{-1}) within branch segments and large rotational jumps (10°–46°) between closely spaced branch segments, and (2) strong crystallographic preferred orientation (CPO) between cpx and titanomagnetite (timt) decorating branch tips, such that $\{010\}_{cpx}$ aligns with one of the six symmetrically equivalent $\{110\}_{timt}$ face poles. More than 80% of timt crystals occur within 5° of the CPO with cpx substrate, as do 22% of timt crystals in contact with euhedral cpx in natural Etna basalt. The probability distribution of distances between an arbitrary unit vector and the nearest $\{110\}_{timt}$ normal unit vector was found by numerical simulation and indicates that the observed alignment to within 5° occurs with frequency 0.024; thus the CPO occurs 9–33 times more commonly than expected from randomly distributed crystals. The CPO matches previous observations of epitaxial relationship between spinel and host pyroxene during subsolidus exsolution, but has not previously been reported among magmatic cpx and timt. Conspicuous contiguity among phenocryst phases is inferred to result from heterogeneous nucleation facilitated by epitaxy associated with CPO, an inference supported by high-resolution electron microscopy observations of 150 nm timt crystals adhering preferentially to silicate substrates. Epitaxial relationships among phases nucleating from a melt may contribute to fabrics in magnetic properties, dictate the textures of igneous rocks by promoting development of crystal clusters, and even influence magma transport and eruption styles through a control over magma rheology.

INTRODUCTION

Crystal clustering, a topic of intensifying investigation in solidifying melts (Day and Taylor, 2007; Ikeda et al., 2002; Jerram and Cheadle, 2000) and aqueous systems (e.g., Banfield et al., 2000), is attributed to processes occurring at a wide range of spatial scales. Monomineralic clusters are attributed to density-driven accumulation, followed by disruption and dispersal as sintered clots into an invading magma (Higgins and Chandrasekharam, 2007; Seaman, 2000), while adhesion of fortuitously impinging grains by a "pressure solution" mechanism (Park and Means, 1996) may explain cognate clusters in magmas of intermediate and mafic composition (e.g., Guilbaud et al., 2007). Clustering of clinopyroxene (cpx) and titanomagnetite (timt) is conspicuous in both phenocryst (Figs. 1A and 1B) and groundmass crystal populations (Fig. 1C; Fig. DR1 in the GSA Data Repository[1]) of oxidized arc magmas. Indeed, clusters composed of mixed mineral phases (e.g., plagioclase, pyroxene, and titanomagnetite) are ubiquitous (Bard, 1986; Williams et al., 1954) and have been attributed to heterogeneous nucleation (Walker et al., 1978) and synneusis, adhesion of crystals in specific orientations that minimize interfacial energy (Schwindinger, 1999; Vance, 1969). It is not yet clear whether crystals more typically cluster upon formation (possibly even prerequisite to formation), or much later as crystals begin to impinge. Recent experimental studies (Ikeda et al., 2002) and simulations (Haxhimali et al., 2006) suggest an important role for crystal-melt and crystal-crystal surface energetics in controlling igneous rock texture. Here we employ backscattered electron (BSE) imaging and the electron backscatter diffraction (EBSD) technique to investigate clinopyroxene-titanomagnetite (cpx-timt) clustering in experimental and natural igneous rocks.

PYROXENE-MAGNETITE CLUSTERING

Dynamic cooling experiments performed under controlled fO_2 conditions on synthetic Fe-rich basalt (described in detail by Hammer, 2006) were conducted from 1210 °C to 300 °C at 3–230 °C h^{-1} with fO_2 fixed at buffers ranging from iron-wüstite to hematite-magnetite. Samples that crystallized at or above the fayalite-magnetite-quartz buffer and ≥19 °C h^{-1} are considered here. The volumetrically dominant phases are cpx ($Wo_7En_{77}Fs_{16}$-$Wo_{39}En_{44}Fs_{17}$), spinel-structured Fe-Ti-Al-Mg oxide ($Fe^{2+}_{0.93}Mg_{0.15}Fe^{3+}_{1.74}Al_{0.10}Ti_{0.08}O_4$-$Fe^{2+}_{1.26}Mg_{0.05}Fe^{3+}_{1.25}Al_{0.13}Ti_{0.31}O_4$) hereafter abbreviated timt, and olivine (Fo_{70-40}). The experiments were designed to emulate likely crystallization environments in the shallow crust of Mars. However,

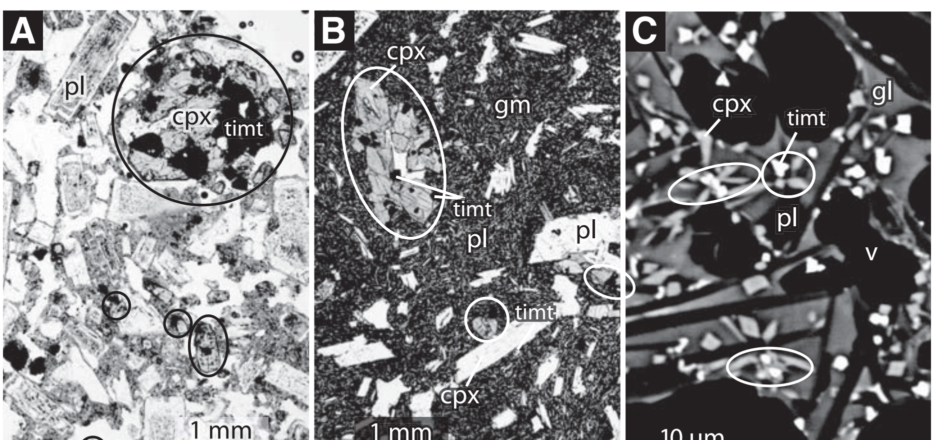

Figure 1. Thin section photomicrographs captured in plane light (A and B) and with backscattered electron imaging (C) illustrating prevalence of cpx-timt contiguity (circled) at a range of spatial scales and two rock types. pl—plagioclase; gm—groundmass; gl—glass; v—vesicle. A: Andesite dome lava from 1995 effusive eruption of Mount Merapi. B and C: Basaltic scoria from the 122 B.C. Plinian eruption of Mount Etna. A less vesicular clast from the Etna deposit (Fig. DR3) proved more amenable to electron backscatter diffraction work (less charging of the uncoated sample).

[1]GSA Data Repository item 2010093, three figures and a description of the EBSD methods, is available online at www.geosociety.org/pubs/ft2010.htm, or on request from editing@geosociety.org or Documents Secretary, GSA, P.O. Box 9140, Boulder, CO 80301, USA.

with respect to kinetic controls on textural development, we regard these runs as being germane to any basalt in which cpx and timt are co-crystallizing phases.

Cpx dendrite branches are conspicuously decorated by timt crystals (Fig. 2A), suggesting timt nucleation on cpx substrate. The fraction of mineral surface area that is shared with another phase may be quantified using contiguity ratios:

$$c_{cpx} = \frac{2N_{cpx\text{-}timt}}{N_{cpx\text{-}matrix} + 2N_{cpx\text{-}timt} + 2N_{cpx\text{-}cpx}}$$

$$c_{timt} = \frac{2N_{cpx\text{-}timt}}{N_{timt\text{-}matrix} + 2N_{cpx\text{-}timt} + 2N_{timt\text{-}timt}}$$

(modified after Gurland, 1968), where "matrix" refers to all other phases, and N values are the quantities of intersections of a specified interface with a randomly oriented test line. For example, $c_{cpx} = 0.14$ in the experimental sample, indicating that 14% of cpx surface area is shared with timt. We evaluate whether the observed contiguity values exceed expectation for randomly distributed crystals by creating separate cpx and timt maps from each base image and then recombining them in random pairings and rotations. The results are cast as the ratio of observed contiguity of phase i (c_i) normalized by the degree of contiguity expected for a random arrangement of the same grains (c_i^o), i.e., $c_i/c_i^o = c_i^n$. This procedure preserves textural attributes (phase area fractions, crystal shape and size) that affect contiguity but would be problematic to simulate numerically. For the experimental sample, $c_{cpx}^n = 1.5$, indicating 50% greater degree of shared cpx surface area than anticipated for randomly oriented cpx and timt crystals.

The c_i^n values thus obtained from the experimental sample and three natural reference samples exhibit a tendency for cpx and timt to share surface area (Table 1). The fraction of shared area is greatest for holocrystalline samples and weakest in glassy samples in which cpx is fine-grained and dispersed. Surface sharing may result from local constitutional undercooling during diffusion-limited crystal growth. Slow-diffusing components rejected by one phase may locally increase the supersaturation of a second phase that requires the rejected components, thus establishing a mutually beneficial relationship between stoichiometrically complementary phases. Alternatively, contiguity could reflect surface energy minimization due to crystallographic alignment of a growing phase on a substrate (i.e., epitaxy). Both mechanisms could develop during early stages of crystal growth, although only the latter is relevant during nucleation.

TABLE 1. CONTIGUITY RATIOS OF EXPERIMENTAL AND NATURAL SAMPLES

Sample	c_{cpx}	c_{cpx}^n	c_{timt}	c_{timt}^n
MA41*	0.14	1.5	0.49	1.2
E3-21†	0.13	1.7	0.22	1.1
E3-27§	0.43	2.5	0.61	1.9
M95c#	0.45	7.3	0.45	4.1

*Experimental sample (Fig. 2A).
†Groundmass crystals in glassy, vesicular Etna basalt (Fig. 1C).
§Groundmass crystals in dense, holocrystalline Etna basalt (Fig. DR1).
#Phenocrysts in Merapi andesite lava (Fig. 1A). Uncertainty (5%) assessed by intrasample heterogeneity.

CRYSTALLOGRAPHIC PREFERRED ORIENTATION

Regions of experimental samples that exhibit conspicuous pyroxene-magnetite contiguity were selected for orientation mapping projects. Region A (Fig. 2A), spanning 2443 µm^2, is composed of glass (62%), cpx (33%), and titanomagnetite (5%). It contains ~100 timt grain intersections and ~50 cpx grain intersections. Region B (679 µm^2; Fig. DR2) is similar, with 63%, 24%, and 9% of these phases, respectively. Indexible diffraction patterns were captured for 44 of the pyroxene intersections in region A and 17 in B. The principal face pole plots for region A (Figs. 2C and 2D) reveal that each grain intersection belongs to one of two distinct crystal lattices and that all pyroxene intersections in region B are part of the same crystal lattice (Figs. DR2C and DR2D). It is not surprising that segmented dendrite arms are connected outside the section plane (O'Driscoll et al., 2007); the EBSD technique vividly demonstrates the magnitude of error that would be introduced if segments were to be considered separate crystals, e.g., for the purpose of nucleation rate determination. A second observation afforded by the upper-hemisphere principal pole plots (Figs. 2C and 2D) is more intriguing. While the $\{010\}_{cpx}$ poles migrate little along the lengths of a given branch, the $\{001\}_{cpx}$ pole rotates about the $\{010\}_{cpx}$ pole up to 170° in a branch that is 80 µm long. That is, the lattices of both curving (region A) and straight cpx crystals (region B) rotate in helical fashion about the b-axis as the crystal grows. Close inspection of individual branches reveals incremental rotations within branch segments (e.g., 0°–0.4° µm^{-1}) and large jumps (e.g., 10°–46°) between adjacent

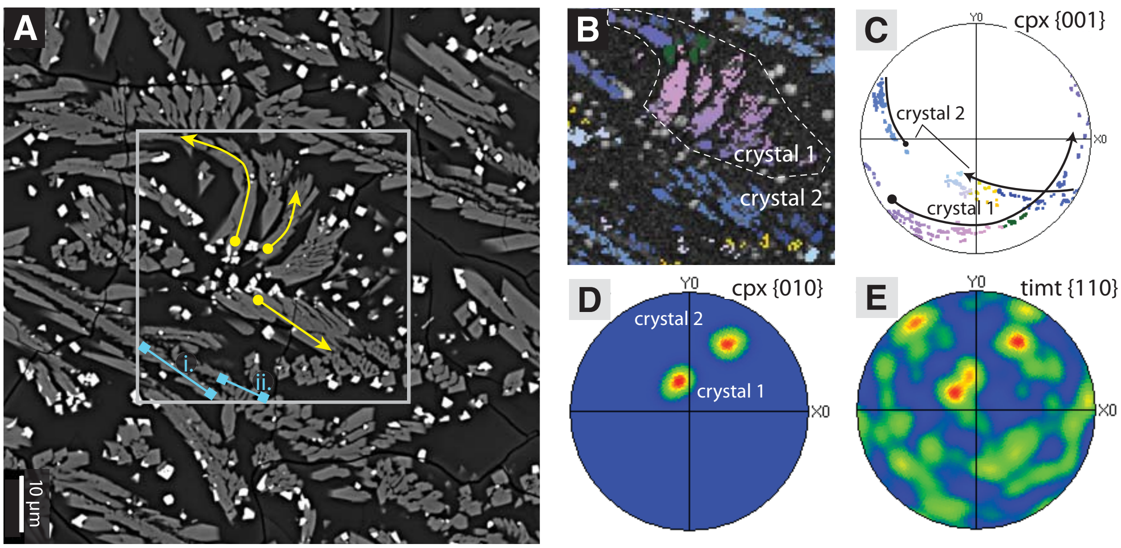

Figure 2. A: Backscattered electron (BSE) image of timt crystals decorating curving cpx dendrites in a glass matrix. The square box indicates region A, discussed in text. Cpx growth direction (yellow arrows) inferred from bifurcation orientation. B: Cpx phase orientation map of region A overlaid on electron backscatter diffraction band contrast image (similar to BSE). Color scheme matches the $\{001\}_{cpx}$ pole figure (C). All colored pixels are attributed to one of two distinct pyroxene lattices, shown in C as two arrays; dashed line in B separates the crystals in the section plane; note crystal 2 surrounds crystal 1. Curved and straight crystals exhibit rotation about $\{010\}_{cpx}$ (C and D), although branch rotation is dominantly accommodated by intersegment jumps. Blue lines i and ii (A), spanning one and six segments, respectively, exhibit $\{010\}_{cpx}$ rotations of 0° and 60° respectively. The $\{010\}_{cpx}$ poles are coincident with $\{110\}_{timt}$ poles, as shown in frequency-contoured face pole plot (E).

segments separated by <1 μm. Third, and most importantly, a strong crystallographic preferred orientation (CPO) exists between cpx and timt, in which the $\{010\}_{cpx}$ pole aligns with one of the six symmetrically equivalent $\{110\}_{timt}$ poles, as revealed in contoured pole figures (Figs. 2D and 2E). In region A, 80% of 44 indexed magnetite crystals are aligned so that one of six$\{110\}_{timt}$ poles falls less than 5° from the {010} pole of the nearest cpx crystal. The percentage of 17 indexed timt crystals in region B exhibiting the CPO with cpx is similar, 82%.

This high degree of CPO frequency is contextualized by comparing the observed angular distribution with the distribution that results from randomly oriented cpx and timt lattices, ascertained by numerical simulation. The angle between a randomly oriented unit vector and the nearest symmetrically equivalent {110} unit vector in the cubic crystal system was measured in 5×10^8 trials. Coincidence of one of the six $\{110\}_{timt}$ poles within 5° of the $\{010\}_{cpx}$ pole occurs in 2.4% of cases (Fig. DR3). Thus, the experimental cpx and timt lattices are aligned 33 times more frequently than are randomly oriented lattices.

We investigated whether contiguous cpx and timt crystals in natural rocks (Fig. 1) manifest the CPO as well. Low-vesicularity pyroclasts from the 122 B.C. eruption of Mount Etna (E128-08; Sable et al., 2006) were selected for EBSD analysis, as they exhibit strong cpx-timt contiguity in both phenocryst and groundmass crystal populations (Figs. 1B, 1C, and DR1; Table 1). The Etna cpx is coarser-grained than experimental cpx, similar in size to timt with which it intergrows, and faceted (thus differing from dendritic experimental crystals in exhibiting interface-limited rather than diffusion-limited crystal growth). The CPO is observed in 22% of 128 touching pairs of groundmass crystals. While this percentage is considerably lower than observed in the experimental samples, it exceeds by a factor of nine the alignment attributed to random chance (Fig. DR3).

DISCUSSION

Crystal growth in a nonstationary liquid may cause dendrite bending in two ways. At high fluid velocities, skin stresses may be sufficient to induce plastic deformation that causes lattice misorientations within and between branch arms (Dragnevski et al., 2002). Alternatively, fluid flow that induces thermal and/or solutal advection provides a thermodynamic impetus for dendrites to turn and grow "upstream" (Chalmers, 1964; Das et al., 2002; Mullis, 1999). However, unlike metal and alloy crystallization in which fluids are stirred in the casting process, the experiments described here are performed in sealed crucibles held in a furnace hot zone having thermal gradient <1° cm^{-1}. Because curvature is prevalent in highly crystalline samples, we speculate that it develops as compositional boundary layers from neighboring branches impinge on one another. Although we were unable to detect compositional gradients by X-ray mapping, they may have existed during dendrite propagation and then relaxed with subsequent cooling. The helical rotation of the crystal lattice is less satisfactorily envisioned. Even crystals that bend during growth in a convecting fluid do not necessarily exhibit rotating lattices (Henry et al., 1998). Crystal lattice rotation is observed in strongly stirred (cast) alloys (Doherty, 2003), and given enough time, surface energy minimization between crystals drives lattice rotation and grain boundary migration (Upmanyu et al., 2006). However, to our knowledge, lattice rotation during growth from a stationary melt has not been reported or modeled. The EBSD technique therefore presents an intriguing opportunity for further study of crystal growth phenomena in geologically relevant materials.

Insights on the CPO are provided by long-recognized subsolidus relationships between these phases. An epitaxial relationship is widely observed in spinel exsolution lamellae within pyroxene (e.g., Feinberg et al., 2004; Okamura et al., 1976), facilitated by similar spacing and plane group symmetries of oxygen atoms of $\{010\}_{cpx}$ and $\{110\}_{timt}$. However, the cpx-timt CPO has apparently never been documented in minerals forming from melt. Its prevalence in both experimental and natural magmas suggests that the surface energy of at least one of these phases is reduced in contact with the other. We conclude that clustering and physical contact of these phases are not likely to depend solely on constitutional supercooling in a boundary layer, but rather develop from heterogeneous nucleation followed by epitaxial crystal growth.

In an attempt to capture incipient co-crystallization, we sought a sample bearing cpx + timt suitable for high-spatial-resolution analysis. Unfortunately, none of the above samples is suitable for characterization at the submicrometer scale. Well-characterized, experimentally crystallized rhyodacite samples (described in Brugger and Hammer, 2010) were selected for their high groundmass crystal number density, fine grain size, and well-constrained thermal history. Pronounced clustering of timt and cpx crystals is evident in all samples examined (e.g., Fig. 3), even for samples containing <1 vol% crystals. Furthermore, although timt-cpx spatial contiguity persists as crystals coarsen, some phenocrysts exhibit a clear antiwetting relationship (Fig. 3C). Cpx-timt avoidance appears to reflect a reversal in the ratio of crystal-crystal surface energy to crystal-melt surface energy, possibly brought about by (1) heterogeneous nucleation and initial epitaxial growth (as postulated above), followed by differential grain rotation and growth in an energetically unfavorable configuration, or (2) impingement of crystals long after nucleation, resulting in random lattice orientations and an energetically unfavorable grain boundary.

CONCLUSIONS

Clinopyroxene and titanomagnetite are clustered in a variety of natural and synthetic rocks, with variable degrees of interface sharing. Not coincidentally, crystallographic lattice preferred orientations between these phases occurs at frequencies far exceeding random chance. Although preliminary, our investigation hints that heterogeneous nucleation plays a role in crystal aggregation in a variety of magma types. The cpx-timt nucleation relationship may have important implications for the magnetic properties of some igneous rocks as well as aspects of magma evolution. For example, if crystal clusters become aligned during magma flow (e.g., Castro et al., 2002) or crystal accumulation (Gee et al., 2004), a preferred orientation relationship of timt crystals may lead to fabrics in magnetic susceptibility (Feinberg et al., 2006), direction, and intensity (Selkin et al., 2000). Clots containing magnetite have higher settling velocities than similarly sized isolated

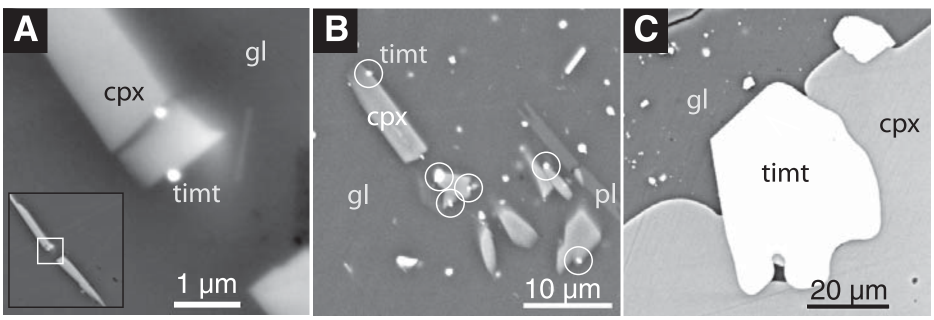

Figure 3. Backscattered electron photomicrographs of titanomagnetite (timt), clinopyroxene (cpx), and plagioclase (pl) co-crystallizing in rhyodacite liquid (gl). Smallest timt crystals are 150 and 450 nm in A and B, respectively. Cpx and timt are distinctly clustered at incipient stages of crystallization (A and B), despite large expanses of melt available for homogeneous nucleation. Some phenocrysts exhibit tendency to minimize crystal-crystal contact area (C).

silicate grains. If clustering is enhanced by the epitaxial relationship as we suggest, heterogeneous timt-cpx crystallization could play a role in crystal layering, with possible consequences for minor and trace element distribution patterns (Boudreau and Philpotts, 2002). Clusters presage extensive networks of touching crystals that control interstitial melt flow as well as igneous rock texture (Jerram et al., 2003). Most intriguingly, cluster-laden magma develops yield strength at lower crystal volume fraction than nonclustered magma of the same particle fraction (Hoover et al., 2001), and thus clusters may influence subsurface magma flow and eruption dynamics. Although the hypothesis demands deeper investigation, the prominence of crystal clusters in the Etna 122 B.C. basalt investigated here may be causally linked with the explosive Plinian eruption style that ejected it.

ACKNOWLEDGMENTS

J. Feinberg, D. Jerram, and an anonymous reviewer are thanked for constructive reviews. We thank S. Sitzman (Oxford Instruments) for electron backscatter (EBSD) expertise on the University of Hawaii instrument, J. Sable and B.F. Houghton for sharing Etna samples, and C. Ma for help with EBSD mapping at the Caltech GPS Analytical Facility. We gratefully acknowledge the use of facilities within the LeRoy Eyring Center for Solid State Science at Arizona State University. This work is supported by National Science Foundation CAREER grant EAR-0449888 to J.E.H. This is School of Ocean and Earth Sciences and Technology publication 7848.

REFERENCES CITED

Banfield, J.F., Welch, S.A., Zhang, H., Ebert, T.T., and Penn, R.L., 2000, Aggregation-based crystal growth and microstructure development in natural iron oxyhydroxide biomineralization products: Science, v. 289, p. 751–754.

Bard, J.P., 1986, Microtextures of igneous and metamorphic rocks: Boston, D. Reidel Publishing Company, 264 p.

Boudreau, A., and Philpotts, A.R., 2002, Quantitative modeling of compaction in the Holyoke flood basalt flow, Hartford Basin, Connecticut: Contributions to Mineralogy and Petrology, v. 144, p. 176–184.

Brugger, C.R., and Hammer, J.E., 2010, Crystallization kinetics in continuous decompression experiments: Implications for interpreting natural magma ascent processes: Journal of Petrology (in press).

Castro, J., Manga, M., and Cashman, K., 2002, Dynamics of obsidian flows inferred from microstructures: Insights from microlite preferred orientations: Earth and Planetary Science Letters, v. 199, p. 211–226.

Chalmers, B., 1964, Principles of solidification: New York, Wiley, 319 p.

Das, A., Ji, S., and Fan, Z., 2002, Morphological development of solidification structures under forced fluid flow: A Monte-Carlo simulation: Acta Materialia, v. 50, p. 4571–4585, doi: 10.1016/S1359-6454(02)00305-1.

Day, J.M.D., and Taylor, L.A., 2007, On the structure of mare basalt lava flows from textural analysis of the LaPaz Icefield and Northwest Africa 032 lunar meteorites: Meteoritics & Planetary Science, v. 42, p. 3–17.

Doherty, R.D., 2003, Comments on "Mechanical deformation of dendrites by fluid flow during solidification of undercooled melts": Scripta Materialia, v. 49, p. 1219–1222, doi: 10.1016/j.scriptamat.2003.08.019.

Dragnevski, K., Mullis, A.M., Walker, D.J., and Cochrane, R.F., 2002, Mechanical deformation of dendrites by fluid flow during the solidification of undercooled melts: Acta Materialia, v. 50, p. 3743–3755, doi: 10.1016/S1359-6454(02)00186-6.

Feinberg, J.M., Wenk, H.-R., Renne, P., and Scott, G.R., 2004, Epitaxial relationships of clinopyroxene-hosted magnetite determined using electron backscatter (EBSD) technique: American Mineralogist, v. 89, p. 462–466.

Feinberg, J.M., Wenk, H.R., Scott, G.R., and Renne, P.R., 2006, Preferred orientation and anisotropy of seismic and magnetic properties in gabbronorites from the Bushveld layered intrusion: Tectonophysics, v. 420, p. 345–356.

Gee, J.S., Meurer, W.P., Selkin, P.A., and Cheadle, M.J., 2004, Quantifying three-dimensional silicate fabrics in cumulates using cumulative distribution functions: Journal of Petrology, v. 45, p. 1983–2009.

Guilbaud, M.N., Blake, S., Thordarson, T., and Self, S., 2007, Role of syn-eruptive cooling and degassing on textures of lavas from the AD 1783–1784 Laki eruption, south Iceland: Journal of Petrology, v. 48, p. 1265–1294, doi: 10.1093/petrology/egm017.

Gurland, J., 1968, Spatial distribution of discrete particles, *in* DeHoff, R.T., and Rhines, F.N., eds., Quantitative Microscopy: New York, McGraw-Hill, p. 278–290.

Hammer, J.E., 2006, Influence of fO_2 and cooling rate on the kinetics and energetics of Fe-rich basalt crystallization: Earth and Planetary Science Letters, v. 248, p. 618–637, doi: 10.1016/j.epsl.2006.04.022.

Haxhimali, T., Karma, A., Gonzales, F., and Rappaz, M., 2006, Orientation selection in dendritic evolution: Nature, v. 5, p. 660–664, doi: 10.1038/nmat1693.

Henry, S., Minghetti, T., and Rappaz, M., 1998, Dendrite growth morphologies in aluminum alloys: Acta Materialia, v. 46, p. 6431–6443, doi: 10.1016/S1359-6454(98)00308-5.

Higgins, M.D., and Chandrasekharam, D., 2007, Nature of sub-volcanic magma chambers, Deccan Province, India: Evidence from quantitative textural analysis of plagioclase megacrysts in the Giant Plagioclase Basalts: Journal of Petrology, v. 48, p. 885–900, doi: 10.1093/petrology/egm005.

Hoover, S.R., Cashman, K.V., and Manga, M., 2001, The yield strength of subliquidus basalts—Experimental results: Journal of Volcanology and Geothermal Research, v. 107, p. 1–18, doi: 10.1016/S0377-0273(00)00317-6.

Ikeda, S., Toriumi, M., Yoshida, H., and Shimizu, I., 2002, Experimental study of the textural development of igneous rocks in the late stage of crystallization: The importance of interfacial energies under non-equilibrium conditions: Contributions to Mineralogy and Petrology, v. 142, p. 397–415.

Jerram, D.A., and Cheadle, M.J., 2000, On the cluster analysis of grains and crystals in rocks: American Mineralogist, v. 85, p. 47–67.

Jerram, D.A., Cheadle, M.J., and Philpotts, A.R., 2003, Quantifying the building blocks of igneous rocks: Are clustered crystal frameworks the foundation?: Journal of Petrology, v. 44, p. 2033–2051, doi: 10.1093/petrology/egg069.

Mullis, A.M., 1999, Growth induced dendritic bending and rosette formation during solidification in a shearing flow: Acta Materialia, v. 47, p. 1783–1789, doi: 10.1016/S1359-6454(99)00052-X.

O'Driscoll, B., Donaldson, C.H., Troll, V.R., Jerram, D.A., and Emeleus, C.H., 2007, An origin for harrisitic and granular olivine in the Rum layered suite, NW Scotland: A crystal size distribution study: Journal of Petrology, v. 48, p. 253–270.

Okamura, F.P., McCallum, I.S., Stroh, J.M., and Ghose, S., 1976, Pyroxene-spinel intergrowths in lunar and terrestrial pyroxenes: Proceedings of the 7th Lunar and Planetary Science Conference, v. 2, p. 1889–1899.

Park, Y., and Means, W.D., 1996, Direct observation of deformation processes in crystal mushes: Journal of Structural Geology, v. 18, p. 847–858, doi: 10.1016/S0191-8141(96)80017-4.

Sable, J.E., Houghton, B.F., Del Carlo, P., and Coltelli, M., 2006, Changing conditions of magma ascent and fragmentation during the Etna 122 BC basaltic Plinian eruption: Evidence from clast microtextures: Journal of Volcanology and Geothermal Research, v. 158, p. 333–354, doi: 10.1016/j.jvolgeores.2006.07.006.

Schwindinger, K.R., 1999, Particle dynamics and aggregation of crystals in a magma chamber with application to Kilauea Iki olivines: Journal of Volcanology and Geothermal Research, v. 88, p. 209–238, doi: 10.1016/S0377-0273(99)00009-8.

Seaman, S.J., 2000, Crystal clusters, feldspar glomerocrysts, and magma envelopes in the Atascosa Lookout lava flow, southern Arizona, USA: Recorders of magmatic events: Journal of Petrology, v. 41, p. 693–716, doi: 10.1093/petrology/41.5.693.

Selkin, P.A., Gee, J.S., Tauxe, L., Meurer, W.P., and Newell, A.J., 2000, The effect of remanence anisotropy on paleointensity estimates: A case study from the Archean Stillwater Complex: Earth and Planetary Science Letters, v. 183, p. 403–416.

Upmanyu, M., Srolovitz, D.J., Lobkovsky, A.E., Warren, J.A., and Carter, W.C., 2006, Simultaneous grain boundary migration and grain rotation: Acta Materialia, v. 54, p. 1707–1719, doi: 10.1016/j.actamat.2005.11.036.

Vance, J.A., 1969, On synneusis: Contributions to Mineralogy and Petrology, v. 24, p. 7–29, doi: 10.1007/BF00398750.

Walker, D., Powell, M.A., Lofgren, G.E., and Hays, J.F., 1978, Dynamic crystallization of a eucrite basalt: Proceedings of the Lunar and Planetary Science Conference, v. 9, p. 1369–1391.

Williams, H., Turner, F.J., and Gilbert, C.M., 1954, Petrography: An introduction to the study of rocks in thin section: San Francisco, Freeman, 406 p.

Manuscript received 6 August 2009
Revised manuscript received 6 November 2009
Manuscript accepted 10 November 2009

Printed in USA